



Structure of avian orthoreovirus virion by electron cryomicroscopy and image reconstruction

Xing Zhang^a, Jinghua Tang^b, Stephen B. Walker^a, David O'Hara^c, Max L. Nibert^{d,*}, Roy Duncan^{c,*}, Timothy S. Baker^{a,b,*}

^aDepartment of Biological Sciences, Purdue University, West Lafayette, IN 47907, USA

^bDepartment of Chemistry and Biochemistry and Department of Molecular Biology, University of California-San Diego, La Jolla, CA 92093, USA

^cDepartment of Microbiology and Immunology, Dalhousie University, Halifax, NS, Canada B3H4H7

^dDepartment of Microbiology and Molecular Genetics, Harvard Medical School, Boston, MA 02115, USA

Received 8 April 2005; returned to author for revision 6 June 2005; accepted 4 August 2005

Abstract

Among members of the genus *Orthoreovirus*, family *Reoviridae*, a group of non-enveloped viruses with genomes comprising ten segments of double-stranded RNA, only the “non-fusogenic” mammalian orthoreoviruses (MRVs) have been studied to date by electron cryomicroscopy and three-dimensional image reconstruction. In addition to MRVs, this genus comprises other species that induce syncytium formation in cultured cells, a property shared with members of the related genus *Aquareovirus*. To augment studies of these “fusogenic” orthoreoviruses, we used electron cryomicroscopy and image reconstruction to analyze the virions of a fusogenic avian orthoreovirus (ARV). The structure of the ARV virion, determined from data at an effective resolution of 14.6 Å, showed strong similarities to that of MRVs. Of particular note, the ARV virion has its pentameric λ -class core turret protein in a closed conformation as in MRVs, not in a more open conformation as reported for aquareovirus. Similarly, the ARV virion contains 150 copies of its monomeric σ -class core-nodule protein as in MRVs, not 120 copies as reported for aquareovirus. On the other hand, unlike that of MRVs, the ARV virion lacks “hub-and-spokes” complexes within the solvent channels at sites of local sixfold symmetry in the incomplete $T = 13I$ outer capsid. In MRVs, these complexes are formed by C-terminal sequences in the trimeric μ -class outer-capsid protein, sequences that are genetically missing from the homologous protein of ARVs. The channel structures and C-terminal sequences of the homologous outer-capsid protein are also genetically missing from aquareoviruses. Overall, the results place ARVs between MRVs and aquareoviruses with respect to the highlighted features.

© 2005 Elsevier Inc. All rights reserved.

Keywords: Orthoreovirus; Reovirus; Reoviridae; Virus structure; Electron cryomicroscopy

Introduction

Electron cryomicroscopy (cryoEM) and three-dimensional image reconstruction (3DR) have been effectively used to determine the arrangements of proteins in the virions and other particle forms of “non-fusogenic” mammalian orthoreoviruses (MRVs), including those of prototype strains type 1 Lang, type 2 Jones, and type 3 Dearing

(T3D) (Metcalf et al., 1991; Dryden et al., 1993, 1998). These methods have proven additionally powerful when combined with fitting of atomic models for the viral proteins derived from recent X-ray crystallographic determinations (Reinisch et al., 2000; Nason et al., 2001; Olland et al., 2001; Liemann et al., 2002; Luongo et al., 2002; Tao et al., 2002; Zhang et al., 2003, in press). This combination of approaches has contributed a number of new conclusions regarding the assembly, disassembly and functions of MRV structural proteins (Liemann et al., 2002; Odegard et al., 2003; Zhang et al., 2003, in press).

MRVs constitute one of at least five species in the genus *Orthoreovirus*, family *Reoviridae*, a group of non-enveloped

* Corresponding authors. Fax: +1 617 738 7664.

E-mail addresses: mnibert@hms.harvard.edu (M.L. Nibert), roy.duncan@dal.ca (R. Duncan), tsb@chem.ucsd.edu (T.S. Baker).

viruses with genomes comprising ten segments of double-stranded (ds) RNA (Duncan, 1999; Duncan et al., 2004). In addition to MRVs, this genus comprises at least four species that induce syncytium formation in cultures of infected cells. These “fusogenic” orthoreoviruses include two isolates from mammals (Nelson Bay virus, from a flying fox, and baboon reovirus) (Gard and Marshall, 1973; Leland et al., 2000) and numerous isolates from different birds and reptiles (Fahey and Crawley, 1954; Gershovitz and Wooley, 1973; McFerran et al., 1976; Ahne et al., 1987; Lamirande et al., 1999; Drury et al., 2002). Sequence comparisons have revealed considerable diversity among the viral species, with levels of amino acid identities between homologous pairs of proteins that range from 16 to 36% (Duncan et al., 2004). As pathogens of poultry (van der Heide, 2000), avian orthoreoviruses (ARVs) hold particular interest for more in-depth studies of the viral particles and proteins.

Although complete genomic sequences have so far been reported only for three MRV strains (Wiener and Joklik, 1989; Breun et al., 2001; Yin et al., 2004), all *Orthoreovirus* species are thought to share a set of seven homologous structural proteins (Table 1), each encoded by a single long open reading frame (ORF) in each of the seven cognate genome segments. This supposition is supported by analysis

of the protein composition of virions and subviral particles of ARV (Schnitzer et al., 1982; Martinez-Costas et al., 1997) as well as by the protein-coding potential of individual genome segments (Varela and Benavente, 1994). Two other monocistronic genome segments in MRVs (segments M3 and S3) and ARVs (segments M3 and S4) encode non-structural proteins (μ NS and σ NS, respectively) that are conserved between these species (Duncan, 1999; Touris-Otero et al., 2004) and probably conserved in the other species as well. The coding capacity of the remaining segment (S1 in MRVs and ARVs) is more variable, comprising two or three distinct ORFs (Nagata et al., 1984; Shapouri et al., 1995; Dawe and Duncan, 2002; Shmulevitz et al., 2002; Duncan et al., 2004). In at least four species, one of these ORFs encodes an eighth structural protein, the fibrous cell-adhesion protein (σ 1 in MRVs, σ C in the fusogenic species) (Nagata et al., 1984; Shapouri et al., 1995; Shmulevitz et al., 2002; Duncan et al., 2004) (Table 1). Baboon reovirus, however, lacks an identifiable homolog of this eighth structural protein (Dawe and Duncan, 2002). In fusogenic species characterized to date, a second ORF in this bi- or tricistronic genome segment encodes the non-structural, fusion-associated small transmembrane (FAST) protein responsible for syncytium formation (Shmulevitz and Duncan, 2000; Dawe and Duncan, 2002; Corcoran and Duncan, 2004).

The family *Reoviridae* currently includes at least eleven additional genera (Mertens, 2004), the members of one of which, *Aquareovirus* (eleven dsRNA genome segments), show clear homologies to MRVs. In fact, the same homologous set of seven structural and two non-structural proteins putatively shared among all orthoreoviruses is also shared among aquareoviruses (Attoui et al., 2002). The virion of striped bass reovirus (SBR), the only aquareovirus yet analyzed by cryoEM and 3DR (at 23-Å resolution), also shows many similarities with that of MRVs (Nason et al., 2000). Some authors have in fact argued that it might be proper to place orthoreoviruses and aquareoviruses within a shared taxonomic group below the family level (Attoui et al., 2002; Kim et al., 2004b), such as in a distinct subfamily or even within the same genus. Interestingly, aquareoviruses share the syncytium-inducing capacity of fusogenic orthoreoviruses (Lupiani et al., 1995), an uncommon property for non-enveloped viruses. In addition to differences in host range (orthoreoviruses have not been isolated from fish), aquareoviruses, or at least SBR, differ from MRVs in a number of structural features, including partially open core turrets in virions (closed in MRVs), 120 core nodules (150 in MRVs), and no fibrous cell-adhesion protein homologous to that of MRVs (Nason et al., 2000).

To date, no cryoEM and 3DR results have been reported for any fusogenic orthoreoviruses. We recognized that such data may be useful to investigate possible divergence of structural features within the genus *Orthoreovirus*, as well as between orthoreoviruses and aquareoviruses. Given increasing attention to molecular and cellular studies of

Table 1

Virion-associated proteins of ARVs, MRVs, and aquareoviruses

Protein homologs		Protein sizes (aa ^a)				Copy no. ^b	Location in virion
ARV	MRV	AqRV ^c	ARV ^d	MRV ^e	AqRV ^f		
λ A	λ I	VP3	1293 ^g	1275	1214	120	Core $T = 1$ shell ^h
λ B	λ J	VP2	NA	1267	1274	~12	Core interior
λ C	λ 2	VP1	1285 ^g	1289	1299	60	Core turrets
μ A	μ 2	VP5	732 ⁱ	736	728	~24	Core interior
μ B	μ 1	VP4	676 ⁱ	708	648	600	Outer $T = 13/$ shell
σ A	σ 2	VP6	416	418	412	150	Core nodules
σ B	σ 3	VP7	367	365	276	600	Surface
σ C	σ 1	–	326	455	–	~36	Surface fiber

^a Total number of amino acids (aa).

^b Values for MRV virions, probably also correct for ARV virions. The values with approximate signs are estimates from best available data for MRV (Coombs, 1998). These values are probably also correct for aquareovirus virions, except that aquareoviruses contain only 120 core nodules formed by VP6 (Nason et al., 2000) and both genetically and structurally lack a σ 1 homolog (Nason et al., 2000; Attoui et al., 2002).

^c AqRV, aquareovirus.

^d Values for ARV strain 138 unless otherwise indicated. GenBank accession numbers in order of listing are AAT27445, AAM46173, AAT52024, AAC18126, AAW78485, AAF45156, and AAC18122; NA, not available.

^e Values for MRV strain T3D. GenBank accession numbers in order of listing are AAD42306, P17378, P11079, AAL99937, M2XR4D, AAA47261, P03527, and P03528.

^f Values for golden shiner reovirus. GenBank accession numbers in order of listing are AAM92746, AAM92745, AAM92744, AAM92748, AAM92749, AAM92752 and AAM92754.

^g Values for ARV-S1133.

^h Because the $T = 1$ shell contains two subunits in each icosahedral asymmetric unit, it is sometimes referred to as “ $T = 2$ ” (Grimes et al., 1998).

ⁱ From Noad et al. (in press).

ARV in the past several years (Hsiao et al., 2002; Shmulevitz et al., 2004; Touris-Otero et al., 2004; Xu et al., 2004), we focused our efforts on one of these fusogenic isolates, ARV-138, a mildly pathogenic strain that grows to high yields in cultured cells and has been the focus of several recent analyses (Duncan and Sullivan, 1998; O'Hara et al., 2001; Patrick et al., 2001).

Results and discussion

CryoEM and image reconstruction of ARV virion

Gradient-purified virions of ARV-138 were visualized by cryoEM as previously described (Baker et al., 1999). Micrographs showed the particles to have a layered capsid morphology typical of the viruses in this genus (Fig. 1A). A 3DR was generated from digitized images of 1086 individual virions obtained from fourteen such micrographs, using established procedures (Baker and Cheng, 1996; Bowman et al., 2002). The data resulting from these procedures showed an effective resolution of 14.6 Å (Fourier shell correlation = 0.5), and the final density map was computed to a resolution limit of 12.1 Å (Fourier shell correlation = 0.143) (Fig. 1B).

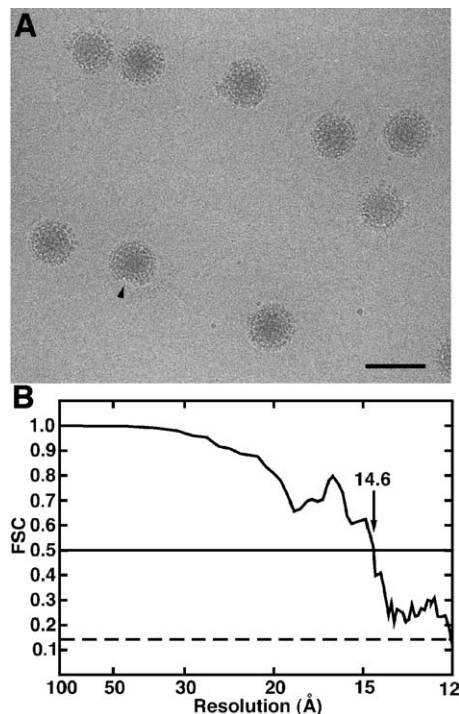


Fig. 1. CryoEM and 3DR of ARV virions. (A) Raw cryoelectron micrograph of well-separated ARV-138 virions. The arrowhead denotes a probable region of degradation in the outer capsid. Scale bar, 100 nm. (B) Plot of the Fourier shell correlation (FSC) as a function of resolution for the averaged electron density map of ARV-138 virions. Based on a conservative threshold criterion (solid horizontal line for FSC = 0.5), the effective resolution of the averaged map is near 14.6 Å. Based on a less stringent noise-limited criterion (dashed horizontal line for FSC = 0.143; Rosenthal and Henderson, 2003), the effective resolution is near 12.1 Å.

Structural comparisons of ARV and MRV virions

Different views of the 3DR of the ARV-138 virion led to an overall conclusion that it shares major structural similarities with that of MRVs, including MRV-T3D (Fig. 2). The overall diameter of the ARV virion, to the top of the major surface protein σ B (Schnitzer et al., 1982; Martinez-Costas et al., 1997), is 857 Å. The previously reported diameter of the MRV virion, to the top of the homologous surface protein σ 3, is ~850 Å (Dryden et al., 1993), or more precisely 854 Å. Neither of these values includes the additional length of the fibrous cell-adhesion protein, σ 1 in MRV or σ C in ARV (Schnitzer et al., 1982; Martinez-Costas et al., 1997), which is poorly visualized by cryoEM and 3DR (Dryden et al., 1993; Chandran et al., 2001; Zhang et al., 2003; this study, see below), but which is known from images of negatively stained samples of MRVs to be capable of extending 400 Å or more from the particle surface (Furlong et al., 1988).

Radially color-coded surface views of the 3DRs of ARV and MRV virions (Figs. 2A, B) revealed several of their similarities. The twelve pentameric core turrets formed by ARV protein λ C (Martinez-Costas et al., 1997), one around each icosahedral fivefold axis, are present in a closed conformation, like the turrets formed by homologous protein λ 2 in MRVs (Metcalf et al., 1991; Dryden et al., 1993). These shared features are also well visualized in central cross-sections of the virions (see Figs. 2C, D). The closed turrets in the ARV and MRV virions contrast with the partially open ones formed by protein VP1 in the virion of aquareovirus SBR (Nason et al., 2000). In MRVs, closure of the turret creates a binding site for the base of cell-adhesion protein σ 1 (Dryden et al., 1993; Chandran et al., 2001), and the same appears true for σ C in ARV. Small “knobs” of density seated above and below λ C directly at each icosahedral fivefold axis (poorly visualized in Fig. 2A, but clearer in Fig. 2C) likely represent small portions of σ C. Interestingly, aquareoviruses lack a genomic σ 1/ σ C homolog, and the SBR virion, for which a 3DR has been determined, lacks a structural σ 1/ σ C analog as well, reflecting its more open turrets. The radial color cueing in Figs. 2A and B makes clear that the tops of the closed turrets (green) are recessed by ~70 Å relative to the rest of the virion surface in both ARV and MRV. Like MRV λ 2, ARV λ C mediates the guanylyltransferase activity and probably also the two methyltransferase activities involved in adding 5' caps to the viral mRNAs as they exit the viral particle following transcription (Martinez-Costas et al., 1995; Hsiao et al., 2002).

On the surface of the ARV virion, in the regions between the turrets, are 600 knobby projections (Fig. 2A) attributable to monomers of the σ B protein. These projections are similar to those formed by the σ 3 protein in MRVs (Metcalf et al., 1991; Dryden et al., 1993; Jané-Valbuena et al., 1999) and are also visualized in the central cross-sections (see Figs. 2C, D). Proteolytic removal of these surface-exposed

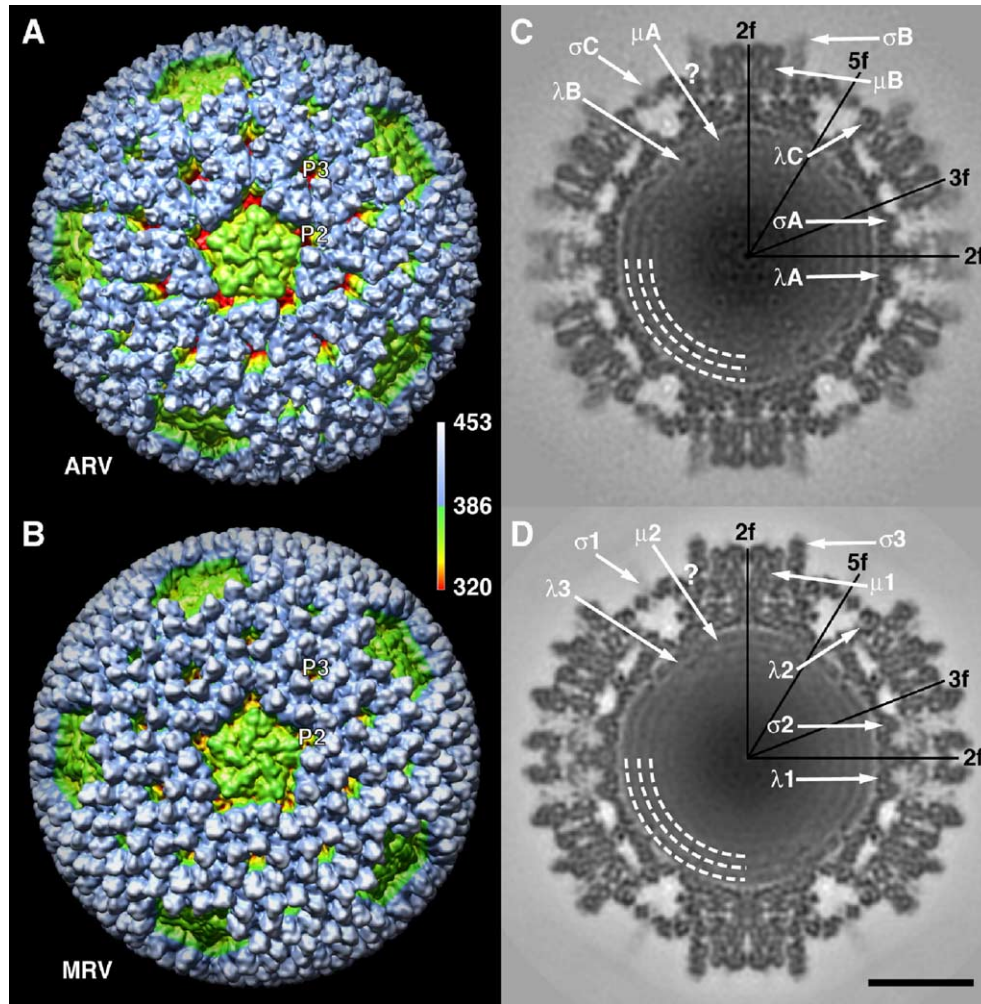


Fig. 2. Surface views and central cross-sections of the 3DRs of ARV and MRV virions. (A, B) Radially color-coded surface views of ARV-138 (A) and MRV-T3D (B). The same radial color map was applied to each particle, as indicated by the legend at right; the numbers indicate radial distances from the center of each particle, in Å. The positions of one P2 channel and one P3 channel are labeled in each particle. (C, D) Central cross-sections of ARV-138 (C) and MRV-T3D (D). Darker shades indicate greater density in the averaged map. Positions of icosahedral twofold (2f), threefold (3f) and fivefold (5f) symmetry are marked by black lines and labeled. Specific densities attributable to each of the seven structural proteins are indicated by white arrows and labeled with the protein names in each particle. Concentric rings of density, attributable to the dsRNA genome segments in the particle interiors, are indicated by curving dashed lines. Scale bar in panel D applies to all panels, 20 nm.

subunits is a required step in cell entry by both ARVs and MRVs (Sturzenbecker et al., 1987; Duncan, 1996). The σ B (or σ 3) monomers are arrayed in groups of either four or six, depending on their positions on the surface (Figs. 2A, B). These arrays surround large solvent conduits, which traverse the full radial width of the outer capsid, are centered at axes of local sixfold symmetry and are comparable to the so-called P2 and P3 channels of MRVs (Metcalf et al., 1991). Arrays of six σ B monomers surround the P3 channels. Arrays of four σ B monomers partially surround the P2 channels, but the other two positions are occupied by parts of the λ C pentamer, similar to the λ 2 pentamer in MRVs (Metcalf et al., 1991; Dryden et al., 1993). In total, 60 P3 and 60 P2 channels are found in the whole outer capsid. The number and arrangement of these channels and the encircling subunits identify the outer capsid of ARV as having incomplete $T = 13$ symmetry, the same as that of

MRVs (Metcalf, 1982; Metcalf et al., 1991). Notably, densities observed in the P3 channels in several previous 3DRs of MRVs (Dryden et al., 1993, 1998; Nason et al., 2001; Zhang et al., in press) are not seen in the current 3DR of ARV, as discussed in detail below.

Central cross-sections of the 3DRs of the ARV and MRV virions (Figs. 2C, D) revealed more of their similarities. Centered at a radius of 268 Å is a largely continuous inner capsid, comparable to that formed by the λ 1 protein in MRVs and thus attributable to the homologous protein λ A in ARV (Martinez-Costas et al., 1997). Inside this layer (i.e., at lower radii) are concentric rings of density, spaced ~ 23 Å apart and attributable to the closely packed genomic dsRNA as in MRVs (Dryden et al., 1993, 1998; Luongo et al., 2002; Zhang et al., 2003). Also inside the λ A shell, along or near each fivefold axis, is some stronger density probably attributable to a portion of the

viral transcriptase complex as in MRVs (Dryden et al., 1998; Zhang et al., 2003). Because of their specific placements and make-ups, the transcriptase complexes located at ten to twelve of the twelve icosahedral fivefold axes per ARV or MRV virion are incompletely visualized in the 3DRs (Figs. 2C, D) but are likely to include the viral RNA-dependent RNA polymerase (protein λ B in ARVs vs. λ 3 in MRVs) as well as the putative polymerase cofactor and nucleoside triphosphate phosphohydrolase (protein μ A in ARVs vs. μ 2 in MRVs) (Schnitzer et al., 1982; Martinez-Costas et al., 1997; Tao et al., 2002; Kim et al., 2004a).

Features reminiscent of the monomeric core nodules and pentameric core turrets of MRVs contact the outside of the λ A shell, at higher radii, in the central cross-sections (Figs. 2C, D). The nodule-like features are comparable to those formed by the σ 2 protein in MRVs and thus attributable to the homologous protein σ A in ARV (Schnitzer et al., 1982; Martinez-Costas et al., 1997). These features are seen in the cross-sections as isolated “bumps”, separated by solvent density, that project upwards from the λ A or λ 1 shell at three distinct positions: surrounding the core turrets (icosahedral fivefold axes), surrounding the icosahedral threefold axes, and across the icosahedral twofold axes

(Figs. 2C, D). The different positions of these σ A or σ 2 nodules are better discerned in radial sections of the 3DRs (see Figs. 3E, F). At their tops, the σ A nodules of ARV contact the major μ -class outer-capsid protein, as do the σ 2 nodules in MRVs (Figs. 2C, D; also see next paragraph). The turret-like features, comparable to those formed by the λ 2 protein in MRVs and attributable to the homologous protein λ C in ARV, are seen in the cross-sections as features that project upwards from the λ A or λ 1 shell and surround a heart-shaped cavity centered along each icosahedral fivefold axis (Figs. 2C, D). This cavity encompasses the path that the nascent viral plus-strand RNAs are thought to travel as they undergo 5'-capping and release from the transcribing viral particle, as in MRVs (Dryden et al., 1993; Reinisch et al., 2000). Also as in MRVs, the turrets are exposed on the virion surface in ARV and thus contribute to the outer capsid. The uppermost portions of each turret (i.e., those at highest radii) run approximately parallel to the particle surface and approach the icosahedral fivefold axis, closing off the top of the turret. The λ C turrets contact all three additional outer-capsid proteins and also contact one of the three types of σ A nodules, as do the λ 2 turrets in MRVs (Figs. 2C, D; also see next paragraph and below). The components described to this point from the cross-sections –

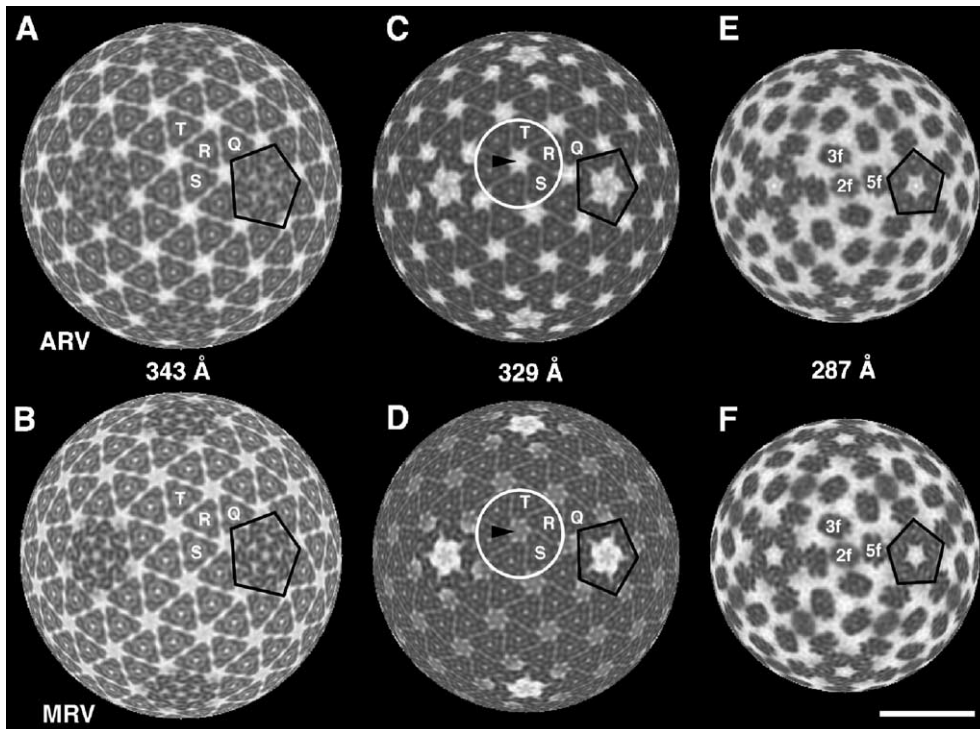


Fig. 3. Radial sections of the 3DRs of ARV and MRV virions. The row of numbers across the middle of the figure indicates the radii, in Å, at which the sectional views above and below each number were generated. Fivefold-symmetrical densities attributable to pentamers of the λ C protein in ARV-138 (A, C, E) or the λ 2 protein in MRV-T3D (B, D, F) are surrounded by a black pentagon in each panel. Threefold-symmetrical densities attributable to trimers of the μ B protein in ARV-138 or the μ 1 protein in MRV-T3D are labeled with white letters in panels A to D; the different letters (Q, R, S, and T) denote the four symmetrically distinct positions that the μ B or μ 1 trimers occupy within the $T = 13$ outer capsid. A region centered on one P3 channel of each particle, and shown in magnified view in Fig. 4, is surrounded by a white circle in panels C and D; arrowheads denote densities in the channel that are absent in ARV-138, but present in MRV-T3D. Ovoid densities attributable to monomers of the σ A protein in ARV-138 or the σ 2 protein in MRV-T3D are labeled with white letters in panels E and F; the different letters (2f, 3f, and 5f) denote the three symmetrically distinct positions that the σ A or σ 2 monomers occupy between the λ 1 (inner) and μ 1 (outer) layers, at or surrounding the icosahedral twofold (2f), threefold (3f), or fivefold (5f) axes. Scale bar in panel F applies to all panels, 20 nm.

dsRNA genome segments and proteins λA , λB , λC , μA , and σA – constitute the ARV core particle (Schnitzer et al., 1982; Martinez-Costas et al., 1997).

The remaining features apparent in the central cross-sections of the ARV and MRV virions (Figs. 2C, D) represent the major parts of the outer capsid. Contacting the sides of the λC turrets as well as the tops of the σA nodules are features comparable to those formed by the $\mu 1$ protein in MRVs and thus attributable to the homologous protein μB in ARV (Schnitzer et al., 1982; Martinez-Costas et al., 1997). Like MRV $\mu 1$, ARV μB is N-terminally myristoylated and is proteolytically cleaved at several discrete sites during assembly or cell entry (Duncan, 1996; Martinez-Costas et al., 1997). Atop the μB densities are additional features comparable to those formed by the $\sigma 3$ protein in MRVs and thus attributable to the homologous protein σB in ARV. The reduced electron density attributable to the σB subunits in this 3DR of ARV virions (Fig. 2C) probably reflects that σB was partially degraded during purification and/or storage prior to microscopy in this study. Lastly, outside the λC turrets along the icosahedral fivefold axes are beads of weak density (poorly visualized in Fig. 2C) comparable to those formed by cell-adhesion protein $\sigma 1$ in MRV and thus likely attributable to the homologous protein, σC , in ARV.

Sectional views at specific radii within viral particles are another effective tool for discerning elements of structure and making comparisons between the particles (Dryden et al., 1993). For example, a comparison of features at a radius of 343 Å in the ARV and MRV virions (Figs. 3A, B) shows remarkable similarities in the densities attributable to proteins λC and μB of ARV and proteins $\lambda 2$ and $\mu 1$ of MRV. Similarly, a comparison of features at a radius of 287 Å in these virions (Figs. 3E, F) shows remarkable similarities in the densities attributable to proteins λC and σA of ARV and proteins $\lambda 2$ and $\sigma 2$ of MRV. Such views strongly support the conclusion that ARV and MRV virions share homologous components and very similar organizations in both inner and outer capsids. On the other hand, some interesting differences are seen near radius 329 Å in the ARV and MRV virions (Figs. 3C, D), as discussed below.

ARV has 150 core nodules

Another major difference between the virions of MRVs and aquareovirus SBR – in addition to whether or not the core turrets are closed and whether or not a cell-adhesion protein is anchored to the top of the turrets (Nason et al., 2000) – concerns the number of core nodules. In SBR, there are 120 core nodules attributed to protein VP6: 60 at sites surrounding the 12 core turrets (icosahedral fivefold axes) and 60 more at sites surrounding the 20 icosahedral threefold axes (Nason et al., 2000). Insect reoviruses from the genus *Cypovirus* also contain 120 such nodules, attributed to protein LPP (Zhou et al., 2003). In MRVs, however, there are 150 core nodules, formed by protein $\sigma 2$:

120 at similar sites as those in SBR and 30 more at sites overlying the 30 icosahedral twofold axes (Dryden et al., 1993; Reinisch et al., 2000). In the ARV virion, as indicated by the central cross-section (Fig. 2C), but more clearly shown by the radial section at 287 Å (Fig. 3E), there are 150 core nodules, attributable to protein σA . Thus, ARV is like MRV and not like SBR in this regard. The slightly smeared density of the twofold nodules apparent in both ARV and MRV virions (Figs. 3E, F) likely reflects that the single σA or $\sigma 2$ subunit at each of these sites can be bound in either of two orientations (Reinisch et al., 2000), which does not reinforce the averaged density to the same high extent as at the other nodule positions, where only one orientation of the σA or $\sigma 2$ subunit is found (Reinisch et al., 2000).

ARV outer capsid lacks hub-and-spokes complexes

The detached spheroidal densities observed in the P3 channels of MRVs in several previous 3DRs (Dryden et al., 1993, 1998; Nason et al., 2001) have been recently visualized as more connected and elaborate “hub-and-spokes” complexes in 3DRs of MRV-T3D at resolutions near 7.0 Å or better (Zhang et al., 2003, in press). Related complexes have been visualized as well in the P2 channels of MRV (Zhang et al., in press), as well as in the P2 and P3 channels of MRV intermediate subvirion particles (X. Zhang, M.A. Agosto, M.L. Nibert, and T.S. Baker, unpublished results). In both locations, the channel structures are attributed to all or part of the C-terminal 33 residues of the major outer-capsid protein $\mu 1$ (Liemann et al., 2002; Odegard et al., 2003; Zhang et al., in press), residues that are disordered and not visible in the X-ray crystal structure of the $\mu 1/\sigma 3$ heterohexamers (Liemann et al., 2002). Whether or not such complexes are present in the ARV virion is somewhat difficult to discern with confidence from the radially color-coded surface view of the whole particle (Fig. 2A), but, in other views, it is clear that such complexes are missing from ARV. For example, the radial sections at 329 Å in the ARV and MRV virions show densities within the P2 and P3 channels of MRV, but not within those of ARV (Figs. 3C, D). This difference is further highlighted by a close-up view of a P3 channel from either virion, across the particle radii at which the hub-and-spokes complex is present in MRV, but not in ARV (Fig. 4). In fact, revisiting the radially color-coded surface view of the whole virions in Figs. 2A and B, one can see that, in the ARV virion, the surfaces of λA and σA (red) are visible through the channels, whereas, in the MRV virion, they are largely obscured by the hub-and-spokes complexes (yellow). The absence of these complexes in ARV-138 is consistent with the fact that the genetically encoded sequence (i.e., ORF) of the $\mu 1$ homolog of ARVs, μB , terminates just before the C-terminal sequences that contribute to forming the hub-and-spokes complexes in MRVs; in sequence alignments, the C-terminal-most encoded residue in μB , Ser676, aligns with $\mu 1$ residue Pro675 (Noad et al., in press) whereas the C-

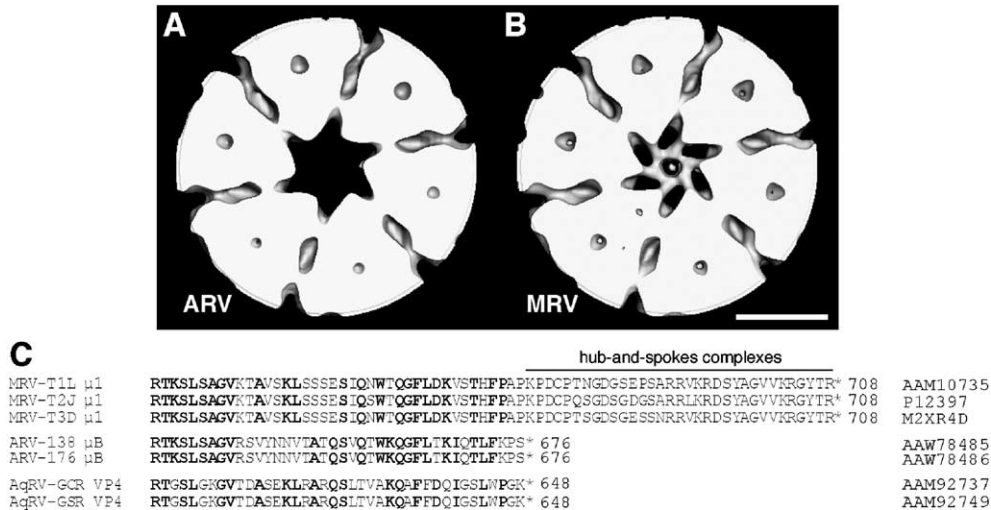


Fig. 4. Magnified views of one P3 channel each from the 3DRs of ARV and MRV virions. The region of each particle shown here is the same as that surrounded by a white circle in Figs. 3C and D. P3 channel densities absent in ARV-138 (A) are present and have a “hub-and-spokes” appearance in MRV-T3D (B). Scale bar in panel B applies to both panels, 1 nm. (C) An alignment of the C-terminal sequences of the homologous $\mu 1$, μB , and VP4 outer-capsid proteins from various isolates of MRV (T1L, type 1 Lang; T2J, type 2 Jones), ARV, and aquareovirus (AqRV) (GCR, grass carp reovirus; GSR, golden shiner reovirus), respectively (Noad et al., in press). Residues identically conserved in at least two of the three groups are bolded. The stop codon that terminates each protein is shown as an asterisk. A GenBank accession number for each sequence is listed at the right.

terminal-most encoded residue in $\mu 1$ is Arg708 (Fig. 4C). Interestingly, the genetically encoded sequence of the $\mu 1/\mu B$ homolog of aquareoviruses, VP4, terminates at the same aligned residue as does μB (Qiu et al., 2001; Liemann et al., 2002), and the SBR virion, for which a 3DR has been determined, also shows no evidence of hub-and-spokes complexes in its P2 or P3 channels (Nason et al., 2000). Thus, ARVs appear to be more similar to aquareoviruses than to MRVs with regard to these features.

ARV outer capsid has $T = 13$ laevo symmetry

Preceding comments about the ARV virion structure do not address the handedness of its capsid lattices. The $T = 13$ outer capsid of MRV virions exhibits laevo handedness (Metcalf, 1982; Dryden et al., 1993). The same is presumably true for the ARV virion, but we did not obtain micrographs from tilted grids in this study that would have allowed us to determine the handedness directly. Instead, we addressed this question by fitting a refined atomic model of the MRV virion (see Materials and methods) into the 3DR of the ARV-138 virion displayed with laevo handedness in its $T = 13$ outer capsid. The extremely good fits that we obtained for nearly all regions or domains of the $\lambda 2$ (Fig. 5A) and $\mu 1$ (Fig. 5C) subunits of MRV within the 3DR of ARV indicate that the outer capsid of the ARV virion does indeed exhibit the same, incomplete $T = 13/1$ symmetry as does that of MRV. In addition, the crystal structure of the $\lambda 2$ pentamer (Reinisch et al., 2000) could be fitted only poorly into the dextro enantiomer of the 3DR of the ARV-138 virion (Fig. 5B). The refined atomic model of the MRV virion fitted into the 3DR of the ARV virion also exhibited close correspondence of features attributable to the $T = 1$

core-shell protein $\lambda 1$ and the core-nodule protein $\sigma 2$ (data not shown). These remarkably similar details of arrangement and shape for the ARV and MRV proteins observed in this experiment thus provide further strong evidence for their major structural similarities.

ARV taxonomy and relation to other reoviruses

In summary, the results of this first 3DR of a fusogenic orthoreovirus, ARV-138, demonstrate strong structural similarities between ARV and non-fusogenic MRV virions, from interior to surface and including many features of both inner and outer capsids. Unique distributions of protein components along different symmetry axes are also shared. Although these strong similarities may have been largely expected from reported protein homologies, the results in this study place structural and functional comparisons of these two most commonly isolated species of the genus *Orthoreovirus* on much firmer ground. Indeed, the many similar details in the ARV and MRV virions observed in this study lead us to conclude with greater confidence that many of the basic functional mechanisms in particle stability, cell entry, mRNA synthesis, and particle assembly are likely to be largely conserved between ARVs and MRVs.

In terms of the evolutionary relationships among ARVs, MRVs, and members of the genus *Aquareovirus*, conformations of the core turrets, numbers of core nodules, and presence or absence of a fibrous cell-adhesion protein homologous to MRV $\sigma 1$ identify ARVs and MRVs as the closer relatives. Other properties such as numbers of genome segments (ten in ARVs and MRVs vs. eleven in aquareoviruses) and levels of sequence identity among the conserved proteins support this conclusion. Notably, in this

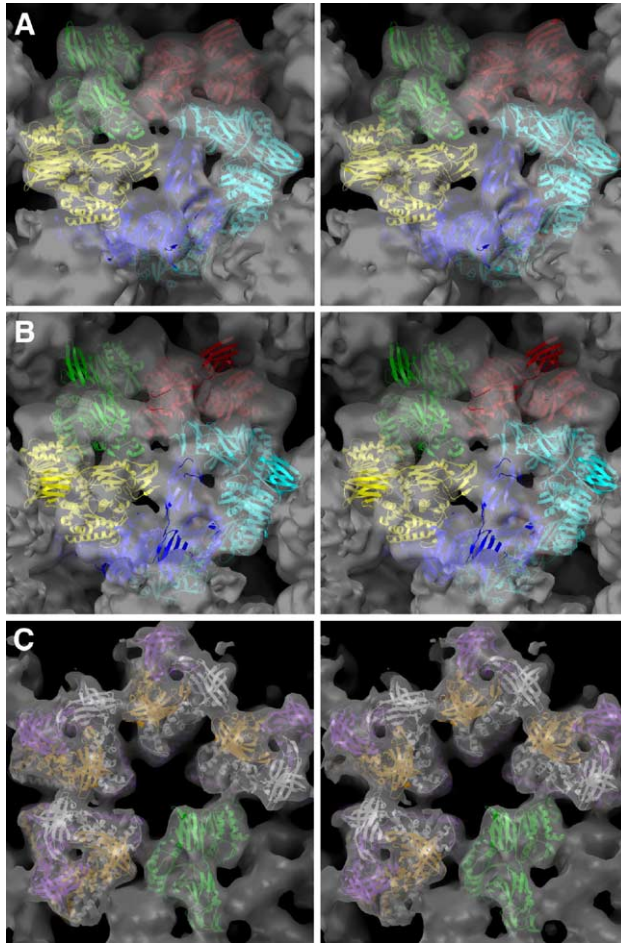


Fig. 5. Stereo views showing fits of the X-ray crystal structures of MRV proteins λ_2 and μ_1 into the 3DR of the ARV virion and its enantiomer. The density map of the ARV-138 virion (gray surface) was rendered with laevo (A, C) or dextro (B) handedness in its $T = 13$ outer capsid. (A, B) The view is centered on the icosahedral fivefold axis. The crystal structure of the λ_2 pentamer (Reinisch et al., 2000) is shown in ribbon format, with each of the five subunits in a different color (green, red, cyan, blue, yellow). Attempts to reposition the λ_2 pentamer within the density map of the dextro enantiomer led, in all instances, to significantly poorer fits than that shown for the laevo enantiomer. (C) The view is centered on a P2 channel adjacent to the icosahedral fivefold axis near the bottom right corner. The crystal structure of the μ_1 trimer (Liemann et al., 2002) is shown in ribbon format, with each of the three subunits in a different color (purple, white, orange), and is fit into each of the four μ_1 trimer positions surrounding the P2 channel. The crystal structure of one adjacent λ_2 subunit is also shown in ribbon format (green).

study, however, we found that ARV-138 is more similar to aquareovirus SBR than to MRVs in lacking hub-and-spokes complexes in its P2 and P3 outer-capsid channels, as formed by C-terminal sequences unique to the μ -class outer-capsid protein of MRVs. Since ARVs and aquareoviruses share syncytium formation in infected cultures as a property that MRVs do not share, it is tempting to speculate that the lack of the channel structures in ARVs and aquareoviruses might represent a covariation that is functionally linked to syncytium formation. However, since the syncytium-inducing p10 protein of ARV is a non-structural protein

(Shmulevitz and Duncan, 2000), it is difficult to envision how or why such a linkage might operate. Another possibility is that the presence or absence of the hub-and-spokes complexes reflects a host-range difference relating to different requirements for particle stability during spread between or within avian or piscine vs. mammalian individuals in the natural world. Further experiments are needed to resolve this question. Structural analysis of the baboon reovirus virion and sequence analysis of its μ -class outer-capsid protein may be informative in this regard since baboon reovirus infects mammals but resembles aquareoviruses in the apparent lack of a $\sigma 1/\sigma C$ -like cell-adhesion protein (Dawe and Duncan, 2002).

Materials and methods

Purifying ARV virions

ARV-138 was grown in QM5 quail fibroblasts as previously described (Duncan and Sullivan, 1998). Viral particles were isolated from the infected cell-culture supernatants by extraction with trichlorotrifluoroethane, ultracentrifugation, and purification on linear CsCl density gradients (1.25 to 1.45 g/cm³) (Duncan, 1996). The well-defined band of virions at a buoyant density of ~ 1.36 g/cm³ was harvested and dialyzed overnight against virion storage buffer (150 mM NaCl, 10 mM MgCl₂, 10 mM Tris, pH 7.5). Gradient-purified virions were stored at 4 °C before use.

Performing cryoEM on ARV virions and determining a 3DR

Gradient-purified ARV-138 virions were embedded in vitreous ice on holey carbon grids maintained at -176 °C and viewed in a Philips CM200 FEG microscope as previously described (Baker et al., 1999). Micrographs were recorded at a nominal magnification of 38,000 \times following low-dose procedures (~ 20 e⁻/Å²). The actual magnification was later determined to be $\sim 38,740\times$ by calibration against an atomic model of the MRV-T3D virion (see below). Micrographs were digitized at 7- μ m intervals on a Zeiss PHODIS scanner, and the data were bin-averaged to obtain pixels corresponding to 3.68 Å in the specimen. Images of 1086 individual particles, well isolated and seemingly intact, were extracted from fourteen scanned micrographs that had been recorded at defocus settings of 0.98 to 4.43 μ m underfocus. A 3DR was generated using established procedures for icosahedral particles (Baker and Cheng, 1996), including corrections by established procedures to compensate in part for effects of the microscope contrast transfer function (Bowman et al., 2002). Orientation angles were evenly distributed throughout the asymmetric unit as shown by all inverse eigenvalues being < 0.01 . The data resulting from these procedures showed an effective resolution of 14.6 Å (Fourier shell correlation = 0.5) (see Fig. 1B). The final

density map was then computed to a resolution limit of 12.1 Å (Fourier shell correlation = 0.143) (see Fig. 1B) by applying an inverse temperature factor of $1/500 \text{ \AA}^2$ to enhance the high-resolution features out to 14.6 Å, after which the inverse factor was held constant, and a Gaussian function was applied to smoothly attenuate the Fourier data to zero amplitude from 14.6 to 12.1 Å.

Displaying 3DRs of the ARV and MRV virions

A previously determined 3DR of the MRV-T3D virion at 7.0-Å resolution (Zhang et al., in press) was used for the comparisons with ARV-138 in this report; however, in order to match the resolution of the ARV map, the MRV map was recomputed in an identical manner as described in the preceding paragraph for ARV. Based on reconstructions of other MRVs (Metcalf et al., 1991; Dryden et al., 1993; X. Zhang, S.B. Walker, M.L. Nibert, and T.S. Baker, unpublished results), the MRV-T3D structure is thought to be representative of all members of that species. All contour-shaded surface views and density-coded (darker, higher density; lighter, lower density) cross-sections and radial sections were generated with RobEM (http://www.bilbo.bio.purdue.edu/~workshop/help_robem/). Radially color-coded surface views were generated with the UCSF Chimera package (<http://www.cgl.ucsf.edu/chimera/>) (Pettersen et al., 2004) from the Computer Graphics Laboratory, University of California, San Francisco (supported by NIH P41 RR-01081). Fig. 1B was prepared by using XMGrace (<http://www.plasma-gate.weizmann.sc.il/Grace/>) and Adobe Illustrator CS. Fig. 5 was prepared by using PMV and VISION (Sanner, 1999; Sanner et al., 2002). All panels in each figure were combined and labeled by using Adobe Photoshop CS.

Fitting crystal structures of MRV proteins into the 3DR of the ARV virion

The pixel size of the MRV-T3D virion reconstruction at 7.0-Å resolution (Zhang et al., in press) was first calibrated against the crystal structure of the reovirus core (Reinisch et al., 2000). The previously reported atomic model of the MRV-T3D virion (Zhang et al., 2003) was then refined against the calibrated MRV-T3D 3DR by use of a real-space procedure contained in the program RSRef (Chapman, 1996). The pixel size of the ARV-138 virion reconstruction at 14.6-Å resolution (this study) was then calibrated, again relative to the crystal structure of the reovirus core. The refined atomic model of the MRV-T3D virion was then fitted into the 3DR of the ARV-138 virion without any further adjustment of individual protein subunits.

Acknowledgments

R.D. expresses his sincere thanks to Jingyun Shou for laboratory support and technical assistance. We also thank

Kevin Coombs for reviewing a draft of the manuscript and for sharing unpublished ARV sequence data for Table 1 and Fig. 4. This work was supported in part by research grants from the National Institutes of Health, USA, to T.S.B. (R37 GM33050) and M.L.N. (R01 AI46440 and R01 AI47904); by research grants from the Canadian Institutes of Health Research and the Natural Sciences and Engineering Research Council, Canada, to R.D.; by shared equipment grant BIR 9112921 from the National Science Foundation, USA, to T.S.B. for purchase of the CM200 FEG microscope; and by a Purdue University reinvestment grant for support of structural biology. S.B.W. was also supported by predoctoral fellowships from the Purdue Research Foundation and from research training grant T32 GM08296 from the National Institutes of Health, USA, to the Biophysics Degree Program at Purdue University. D.O. was also supported by a predoctoral fellowship from the Natural Sciences and Engineering Research Council, Canada. R.D. is the recipient of a Canadian Institutes of Health Research-Regional Partnership Program Investigator Award.

References

- Ahne, W., Thomsen, I., Winton, J., 1987. Isolation of a reovirus from the snake, *Python regius* (Brief Report). Arch. Virol. 94, 135–139.
- Attoui, H., Fang, Q., Jaafar, F.M., Cantaloube, J.F., Biagini, P., De Micco, P., De Lamballerie, X., 2002. Common evolutionary origin of aquareoviruses and orthoreoviruses revealed by genome characterization of Golden shiner reovirus, Grass carp reovirus, Striped bass reovirus and golden ide reovirus (genus *Aquareovirus*, family *Reoviridae*). J. Gen. Virol. 83, 1941–1951.
- Baker, T.S., Cheng, R.H., 1996. A model-based approach for determining orientations of biological macromolecules imaged by cryo-electron microscopy. J. Struct. Biol. 116, 120–130.
- Baker, T.S., Olson, N.H., Fuller, S.D., 1999. Adding the third dimension to virus life cycles: three-dimensional reconstruction of icosahedral viruses from cryo-electron micrographs. Microbiol. Mol. Biol. Rev. 63, 862–922.
- Bowman, V.D., Chase, E.S., Franz, A.W.E., Chipman, P.R., Zhang, X., Perry, K.L., Baker, T.S., Smith, T.J., 2002. An antibody to the putative aphid recognition site on cucumber mosaic virus recognizes pentons but not hexons. J. Virol. 76, 12250–12258.
- Breun, L.A., Broering, T.J., McCutcheon, A.M., Harrison, S.J., Luongo, C.L., Nibert, M.L., 2001. Mammalian reovirus L2 gene and $\lambda 2$ core spike protein sequences and pangenomic comparisons of reoviruses type 1 Lang, type 2 Jones, and type 3 Dearing. Virology 287, 333–348.
- Chandran, K., Zhang, X., Olson, N.O., Walker, S.B., Chappell, J.D., Dermody, T.S., Baker, T.S., Nibert, M.L., 2001. Complete in vitro assembly of the reovirus outer capsid produces highly infectious particles suitable for genetic studies of the receptor-binding protein. J. Virol. 75, 5335–5342.
- Chapman, M.S., 1996. Structural refinement of the DNA-containing capsid of canine parvovirus using RSRef, a resolution-dependent stereochemically restrained real-space refinement method. Acta Crystallogr., Sect. D: Biol. Crystallogr. 52, 129–142.
- Coombs, K.M., 1998. Stoichiometry of reovirus structural proteins in virus, ISVP, and core particles. Virology 243, 218–228.
- Corcoran, J.A., Duncan, R., 2004. Reptilian reovirus utilizes a small type III protein with an external myristoylated amino terminus to mediate cell–cell fusion. J. Virol. 78, 4342–4351.
- Dawe, S., Duncan, R., 2002. The S4 genome segment of baboon reovirus is

- bicistronic and encodes a novel fusion-associated small transmembrane protein. *J. Virol.* 76, 2131–2140.
- Drury, S.E., Gough, R.E., Welchman Dde, B., 2002. Isolation and identification of a reovirus from a lizard, *Uromastyx hardwickii*, in the United Kingdom. *Vet. Rec.* 151, 637–638.
- Dryden, K.A., Wang, G., Yeager, M., Nibert, M.L., Coombs, K.M., Furlong, D.B., Fields, B.N., Baker, T.S., 1993. Early steps in reovirus infection are associated with dramatic changes in supramolecular structure and protein conformation: analysis of virions and subviral particles by cryoelectron microscopy and image reconstruction. *J. Cell Biol.* 122, 1023–1041.
- Dryden, K.A., Farsetta, D.L., Wang, G., Keegan, J.M., Fields, B.N., Baker, T.S., Nibert, M.L., 1998. Internal structures containing transcriptase-related proteins in top component particles of mammalian orthoreovirus. *Virology* 245, 33–46.
- Duncan, R., 1996. The low pH-dependent entry of avian reovirus is accompanied by two specific cleavages of the major outer capsid protein μ 2C. *Virology* 219, 179–189.
- Duncan, R., 1999. Extensive sequence divergence and phylogenetic relationships between the fusogenic and nonfusogenic orthoreoviruses: a species proposal. *Virology* 260, 316–328.
- Duncan, R., Sullivan, K., 1998. Characterization of two avian reoviruses that exhibit strain-specific quantitative differences in their syncytium-inducing and pathogenic capabilities. *Virology* 250, 263–272.
- Duncan, R., Corcoran, J., Shou, J., Stoltz, D., 2004. Reptilian reovirus: a new fusogenic orthoreovirus species. *Virology* 319, 131–140.
- Fahey, J.E., Crawley, J.F., 1954. Studies on chronic respiratory disease of chickens: II. Isolation of a virus. *Can. J. Comp. Med.* 18, 13–21.
- Furlong, D.B., Nibert, M.L., Fields, B.N., 1988. Sigma 1 protein of mammalian reoviruses extends from the surfaces of viral particles. *J. Virol.* 62, 246–256.
- Gard, G.P., Marshall, I.D., 1973. Nelson Bay virus. A novel reovirus. *Arch. Gesamte Virusforsch.* 43, 34–42.
- Gershowitz, A., Wooley, R.E., 1973. Characterization of two reoviruses isolated from turkeys with infectious enteritis. *Avian Dis.* 17, 406–414.
- Grimes, J.M., Burroughs, J.N., Gouet, P., Diprose, J.M., Malby, R., Zientara, S., Mertens, P.P.C., Stuart, D.I., 1998. The atomic structure of the bluetongue virus core. *Nature* 395, 470–478.
- Hsiao, J., Martinez-Costas, J., Benavente, J., Vakharia, V.N., 2002. Cloning, expression, and characterization of avian reovirus guanylyltransferase. *Virology* 296, 288–299.
- Jané-Valbuena, J., Nibert, M.L., Spencer, S.M., Walker, S.B., Baker, T.S., Chen, Y., Centonze, V.E., Schiff, L.A., 1999. Reovirus virion-like particles obtained by recoating infectious subviral particles with baculovirus-expressed σ 3 protein: an approach for analyzing σ 3 functions during virus entry. *J. Virol.* 73, 2963–2973.
- Kim, J., Parker, J.S.L., Murray, K.E., Nibert, M.L., 2004a. Nucleoside and RNA triphosphatase activities of Orthoreovirus transcriptase cofactor μ 2. *J. Biol. Chem.* 279, 4394–4403.
- Kim, J., Tao, Y., Reinisch, K.M., Harrison, S.C., Nibert, M.L., 2004b. Orthoreovirus and Aquareovirus core proteins: conserved enzymatic surfaces, but not protein–protein interfaces. *Virus Res.* 101, 15–28.
- Lamirande, E.W., Nichols, D.K., Owens, J.W., Gaskin, J.M., Jacobson, E.R., 1999. Isolation and experimental transmission of a reovirus pathogenic in ratsnakes (*Elaphe species*). *Virus Res.* 63, 135–141.
- Leland, M.M., Hubbard, G.B., Sentmore III, H.T., Soike, K.F., Hilliard, J.K., 2000. Outbreak of Orthoreovirus-induced meningoencephalomyelitis in baboons. *Comp. Med.* 50, 199–205.
- Liemann, S., Chandran, K., Baker, T.S., Nibert, M.L., Harrison, S.C., 2002. Structure of the reovirus membrane-penetration, μ 1, in a complex with its protector protein, σ 3. *Cell* 108, 283–295.
- Luongo, C.L., Zhang, X., Walker, S.B., Chen, Y., Broering, T.J., Farsetta, D.L., Bowman, V.D., Baker, T.S., Nibert, M.L., 2002. Loss of activities for mRNA synthesis accompanies loss of λ 2 spikes from reovirus cores: an effect of λ 2 on λ 1 shell structure. *Virology* 296, 24–38.
- Lupiani, B., Subramanian, K., Samal, S.K., 1995. Aquareoviruses. *Annu. Rev. Fish Dis.* 5, 175–208.
- Martinez-Costas, J., Varela, R., Benavente, J., 1995. Endogenous enzymatic activities of the avian reovirus S1133: identification of the viral capping enzyme. *Virology* 206, 1017–1026.
- Martinez-Costas, J., Grande, A., Varela, R., Garcia-Martinez, C., Benavente, J., 1997. Protein architecture of avian reovirus S1133 and identification of the cell attachment protein. *J. Virol.* 71, 59–64.
- McFerran, J.B., Connor, T.J., McCracken, R.M., 1976. Isolation of adenoviruses and reoviruses from avian species other than domestic fowl. *Avian Dis.* 20, 519–524.
- Mertens, P., 2004. The dsRNA viruses. *Virus Res.* 101, 3–13.
- Metcalf, P., 1982. The symmetry of the reovirus outer shell. *J. Ultrastruct. Res.* 78, 292–301.
- Metcalf, P., Cyrklaff, M., Adrian, M., 1991. The three-dimensional structure of reovirus obtained by cryo-electron microscopy. *EMBO J.* 10, 3129–3136.
- Nagata, L., Masri, S.A., Mah, D.C., Lee, P.W.K., 1984. Molecular cloning and sequencing of the reovirus (serotype 3) S1 gene which encodes the viral cell attachment protein σ 1. *Nucleic Acids Res.* 12, 8699–8710.
- Nason, E.L., Samal, S.K., Prasad, B.V.V., 2000. Trypsin-induced structural transformation in aquareovirus. *J. Virol.* 74, 6546–6555.
- Nason, E.L., Wetzel, J.D., Mukherjee, S.K., Barton, E.S., Prasad, B.V.V., Dermody, T.S., 2001. A monoclonal antibody specific for reovirus outer-capsid protein σ 3 inhibits σ 1-mediated hemagglutination by steric hindrance. *J. Virol.* 75, 6625–6634.
- Noad, L., Shou, J., Coombs, K.M., Duncan, R., in press. Sequences of avian reovirus M1, M2, and M3 genes and structure/function of the encoded λ μ proteins. *Virus Res.*
- O'Hara, D., Patrick, M., Cepica, D., Coombs, K.M., Duncan, R., 2001. Avian reovirus major m-class outer capsid protein influences efficiency of productive macrophage infection in a virus strain-specific manner. *J. Virol.* 75, 5027–5035.
- Odegard, A.L., Chandran, K., Liemann, S., Harrison, S.C., Nibert, M.L., 2003. Disulfide bonding among μ 1 trimers in mammalian reovirus outer capsid: a late and reversible step in virion morphogenesis. *J. Virol.* 77, 5389–5400.
- Olland, A.M., Jané-Valbuena, J., Schiff, L.A., Nibert, M.L., Harrison, S.C., 2001. Structure of the reovirus outer capsid and dsRNA-binding protein σ 3 at 1.8 Å resolution. *EMBO J.* 20, 979–989.
- Patrick, M., Duncan, R., Coombs, K.M., 2001. Generation and genetic characterization of avian reovirus temperature-sensitive mutants. *Virology* 284, 113–122.
- Pettersen, E.F., Goddard, T.D., Huang, C.C., Couch, G.S., Greenblatt, D.M., Meng, E.C., Ferrin, T.E., 2004. UCSF Chimera—A visualization system for exploratory research and analysis. *J. Comput. Chem.* 25, 1605–1612.
- Qiu, T., Lu, R.H., Zhang, J., Zhu, Z.Y., 2001. Molecular characterization and expression of the M6 gene of grass carp hemorrhage virus (GCHV), an aquareovirus. *Arch. Virol.* 146, 1391–1397.
- Reinisch, K.M., Nibert, M.L., Harrison, S.C., 2000. Structure of the reovirus core at 3.6 Å resolution. *Nature* 404, 960–967.
- Rosenthal, P.B., Henderson, R., 2003. Optimal determination of particle orientation, absolute hand, and contrast loss in single-particle electron cryomicroscopy. *J. Mol. Biol.* 333, 721–745.
- Sanner, M.F., 1999. Python: a programming language for software integration and development. *J. Mol. Graphics Mod.* 17, 57–61.
- Sanner, M.F., Stoffer, D., Olson, A.J., 2002. ViPER, A Visual Programming Environment for Python. Proceedings of the 10th International Python Conference, pp. 103–115.
- Schnitzer, T., Ramos, T., Gouvea, V., 1982. Avian reovirus polypeptides: analysis of intracellular virus specified products, virions, top component, and cores. *J. Virol.* 43, 1006–1014.
- Shapouri, M.R., Kane, M., Letarte, M., Bergeron, J., Arella, M., Silim, A., 1995. Cloning, sequencing and expression of the S1 gene of avian reovirus. *J. Gen. Virol.* 76, 1515–1520.
- Shmulevitz, M., Duncan, R., 2000. A new class of fusion-associated small transmembrane (FAST) proteins encoded by the nonenveloped fusogenic reoviruses. *EMBO J.* 19, 902–912.

- Shmulevitz, M., Yameen, Z., Dawe, S., Shou, J., O'Hara, D., Holmes, I., Duncan, R., 2002. Sequential partially overlapping gene arrangement in the tricistronic S1 genome segments of avian reovirus and Nelson Bay reovirus: implications for translation initiation. *J. Virol.* 76, 609–618.
- Shmulevitz, M., Corcoran, J., Salsman, J., Duncan, R., 2004. Cell–cell fusion induced by the avian reovirus membrane fusion protein is regulated by protein degradation. *J. Virol.* 78, 5996–6004.
- Sturzenbecker, L.J., Nibert, M., Furlong, D., Fields, B.N., 1987. Intracellular digestion of reovirus particles requires a low pH and is an essential step in the viral infectious cycle. *J. Virol.* 61, 2351–2361.
- Tao, Y., Farsetta, D.L., Nibert, M.L., Harrison, S.C., 2002. RNA synthesis in a cage—Structural studies of the reovirus polymerase $\lambda 3$. *Cell* 111, 733–745.
- Touris-Otero, F., Martinez-Costas, J., Vakharia, V.N., Benavente, J., 2004. Avian reovirus nonstructural protein mNS forms viroplasm-like inclusions and recruits protein μ NS to these structures. *Virology* 319, 94–106.
- van der Heide, L., 2000. The history of avian reovirus. *Avian Dis.* 44, 638–641.
- Varela, R., Benavente, J., 1994. Protein coding assignment of avian reovirus strain S1133. *J. Virol.* 68, 6775–6777.
- Wiener, J.R., Joklik, W.K., 1989. The sequences of the reovirus serotype 1, 2, and 3 L1 genome segments and analysis of the mode of divergence of the reovirus serotypes. *Virology* 169, 194–203.
- Xu, W., Patrick, M.K., Hazelton, P.R., Coombs, K.M., 2004. Avian reovirus temperature-sensitive mutant tsA12 has a lesion in major core protein σA and is defective in assembly. *J. Virol.* 78, 11142–11151.
- Yin, P., Keirstead, N.D., Broering, T.J., Arnold, M.M., Parker, J.S.L., Nibert, M.L., Coombs, K.M., 2004. Comparisons of the M1 genome segments and encoded $\mu 2$ proteins of different reovirus isolates. *Virol. J.* 1, 6.
- Zhang, X., Walker, S.B., Chipman, P.R., Nibert, M.L., Baker, T.S., 2003. Reovirus polymerase $\lambda 3$ localized by cryo-electron microscopy of virions at a resolution of 7.6 Å. *Nat. Struct. Biol.* 10, 1011–1018.
- Zhang, X., Ji, Y., Zhang, L., Harrison, S.C., Marinescu, D.C., Nibert, M. L., Baker, T.S., in press. Features of Reovirus Outer-Capsid Protein $\mu 1$ Revealed by Electron Cryomicroscopy and Image Reconstruction of the Virion at 7.0-Å Resolution. *Structure*. 13.
- Zhou, Z.H., Zhang, H., Jakana, J., Lu, X.Y., Zhang, J.Q., 2003. Cytoplasmic polyhedrosis virus structure at 8 Å by electron cryomicroscopy: structural basis of capsid stability and mRNA processing regulation. *Structure* 11, 651–663.